



NIH PUBLIC ACCESS

Author Manuscript

J Magn Magn Mater. Author manuscript; available in PMC 2011 March 1.

Published in final edited form as:

J Magn Magn Mater. 2010 March 1; 322(6): 727–733. doi:10.1016/j.jmmm.2009.10.050.

Heating in the MRI environment due to superparamagnetic fluid suspensions in a rotating magnetic field

P. Cantillon-Murphy^{a,b}, L.L. Wald^c, E. Adalsteinsson^{b,c}, and M. Zahn^b

P. Cantillon-Murphy: padraig@mit.edu; L.L. Wald: wald@nmr.mgh.harvard.edu; E. Adalsteinsson: elfar@mit.edu; M. Zahn: zahn@mit.edu

^aDepartment of Gastroenterology, Brigham and Women's Hospital, Boston, MA.^bDepartment of Electrical Engineering and Computer Science, Massachusetts Institute of Technology, Cambridge, MA.^cMGH-HST Athinoula A. Martinos Center for Biomedical Imaging, Charlestown, MA.

Abstract

In the presence of alternating-sinusoidal or rotating magnetic fields, magnetic nanoparticles will act to realign their magnetic moment with the applied magnetic field. The realignment is characterized by the nanoparticle's time constant, τ . As the magnetic field frequency is increased, the nanoparticle's magnetic moment lags the applied magnetic field at a constant angle for a given frequency, Ω , in rad/s. Associated with this misalignment is a power dissipation that increases the bulk magnetic fluid's temperature which has been utilized as a method of magnetic nanoparticle hyperthermia, particularly suited for cancer in low-perfusion tissue (e.g., breast) where temperature increases of between 4°C and 7°C above the ambient *in vivo* temperature cause tumor hyperthermia. This work examines the rise in the magnetic fluid's temperature in the MRI environment which is characterized by a large DC field, B_0 . Theoretical analysis and simulation is used to predict the effect of both alternating-sinusoidal and rotating magnetic fields transverse to B_0 . Results are presented for the expected temperature increase in small tumors (~1 cm radius) over an appropriate range of magnetic fluid concentrations (0.002 to 0.01 solid volume fraction) and nanoparticle radii (1 to 10 nm). The results indicate that significant heating can take place, even in low-field MRI systems where magnetic fluid saturation is not significant, with careful selection of the rotating or sinusoidal field parameters (field frequency and amplitude). The work indicates that it may be feasible to combine low-field MRI with a magnetic hyperthermia system using superparamagnetic iron oxide nanoparticles.

Keywords

Hyperthermia; magnetic nanoparticles; MRI; heating; superparamagnetic fluids

© 2009 Elsevier B.V. All rights reserved.

Correspondence to: P. Cantillon-Murphy, padraig@mit.edu.

Publisher's Disclaimer: This is a PDF file of an unedited manuscript that has been accepted for publication. As a service to our customers we are providing this early version of the manuscript. The manuscript will undergo copyediting, typesetting, and review of the resulting proof before it is published in its final citable form. Please note that during the production process errors may be discovered which could affect the content, and all legal disclaimers that apply to the journal pertain.

1 Introduction

Recent years have seen the development of an entire field of research dedicated to the treatment of cancer patients, based on the localized heating effects of magnetic nanoparticles *in vivo* [1,2,4–6]. Treatment falls under one of two categories, hyperthermia and thermoablation.

In hyperthermia, the target area is subjected to a local temperature in the range of 42°C to 45°C for periods of up to a few hours [4]. This temperature range is destructive to cancerous cells without harming healthy cells. The end result is usually not sufficient to eradicate all the cancerous cells and is coupled with other techniques such as irradiation or chemotherapy [6]. Thermoablation aims at creating *in vivo* temperatures in excess of 50° in the tumor region and exposure time is limited to just minutes. Although this approach would appear preferred, there are concerns regarding the physiological effects of such a rapid, localized heating effect [7]. To date, particles that have been used are either injected *in situ* or are designed to bind selectively to cancerous cells. The majority of investigations use superparamagnetic magnetite (Fe_3O_4) or maghemite ($\gamma\text{-Fe}_2\text{O}_3$) in water based suspensions since these are well metabolized. Creating *in vivo* concentrations to allow for sufficient heating is a major challenge due to heat conduction away from the target area as well as blood perfusion around the tumor [4]. A second significant challenge is the undesired heating associated with eddy currents in surrounding healthy tissue [8]. Brezovich [8] found that “subjects had a sensation of warmth but were able to withstand the treatment for more than an hour” when the product of the field amplitude H_e and the frequency $f = \Omega/(2\pi)$ did not exceed 4.85×10^8 (A/m)/s. Superparamagnetic particles of magnetite and maghemite have been the preferred nanoparticle to date [5] but recent developments such as FeCo particles [9] would offer significant advantage due to the increased magnetic moment per particle if concerns regarding biocompatibility can be overcome.

Rosensweig [2] examined the heating effect of alternating-sinusoidal RF fields on superparamagnetic fluid suspensions. His work developed dissipation relationships based on the rotational relaxation of single-domain magnetic nanoparticles dispersed in a tetradecane solvent due to sinusoidal magnetic fields. Eddy current heating due to ohmic dissipation is assumed to be negligible due to the small size of the particles (< 20 nm core diameter) compared to the skin depth. Rosensweig expressed the volumetric power dissipation using a simplified version of Shliomis’ Relaxation Equation [17] in the absence of so-called “spin-velocity” effects for a magnetic fluid suspension in an alternating-sinusoidal RF field. This present work follows Rosensweig’s approach and introduces two new significant developments: (i) the analysis is revised for the presence of rotating as well as alternating-sinusoidal magnetic fields and (ii) the analysis is examined in the MRI environment, where, it is expected that the heating effect will be limited due to the magnetic fluid approaching saturation in the presence of the large DC magnetic field, denoted B_0 , characteristic of MRI. The notion of a combined MRI/hyperthermia unit has existed for some time [10,11] using RF ablation techniques. This work represents the first known analytical study accounting for both magnetic saturation effects due to the MRI and the heating effects of superparamagnetic nanoparticles in a rotating field, for purposes of hyperthermia treatment.

2 Theory

The analysis is performed in two distinct phases. Firstly, the fluid magnetization is solved as a function of all the variables of interest following and extending Rosensweig’s approach [2]. Next, the resultant temperature increase in low perfusion tissue is solved using established results for heat conduction from a spherical volume (representing a small tumor) with uniform heat generation (due to the heating effect of the magnetic nanoparticles in the rotating magnetic field) to the surrounding medium (see Carslaw and Jaeger,[3] pp.232), in a similar manner to the results obtained by Andra et al. [18].

2.1 Magnetic Relaxation

The governing equation on a magnetic fluid's equilibrium magnetization, \mathbf{M}_{eq} , in a magnetic field is the Langevin Relation [1] given by (1) and (2).

In the presence of either alternating-sinusoidal or rotating magnetic fields, the fluid's magnetization is governed by:

- i. the conservation of linear momentum given by (3) in the absence of pressure differentials and neglecting inertia [15]
- ii. the conservation of angular momentum (4) neglecting spin viscosity and inertia [15]
- iii. Shliomis' Relaxation Equation [17], given by (5), which governs magnetic relaxation of the superparamagnetic nanoparticles.

In general, the Langevin relation determines the extent of magnetic saturation of the nanoparticles in the suspension. This depends on the strength of the applied field. Two fields are considered in this work, one either alternating-sinusoidal or rotating in the transverse xy plane and the second, the large z -directed DC B_0 field associated with the MRI. In the absence of B_0 , the Langevin function will be determined by the "chord susceptibility", following Rosensweig's approach [2]. In the presence of both transverse and z -directed fields, only B_0 will be considered in determining the Langevin relation since, for the analysis which follows, the alternating-sinusoidal or rotating fields do not exceed 10% of B_0 , when it is present. Therefore, the z -directed component of the equilibrium magnetization, \mathbf{M}_{eq} , is denoted M_0 , and in the presence of a z -directed, DC magnetic field with magnitude H_0 , is given by (1) where

$\alpha = \frac{\mu_0 V_p M_d H_0}{kT}$ and $M_0 \ll H_0$ for large field strengths ($\mu_0 H_0 > 0.1$ T). The nanoparticle magnetic volume is V_p , the single-domain magnetization, M_d (assumed that of magnetite in the results which follow, with a value of 446 kA/m) and the thermal energy density is kT . The saturation magnetization, $M_s = \phi M_d$, where ϕ is the fraction solid magnetic volume in the magnetic fluid suspension.

$$\mathbf{M}_{eq} = \mathbf{M}_s L(\alpha) = \mathbf{M}_s (\coth(\alpha) - 1/\alpha) \quad (1)$$

$$\alpha = \frac{\mu_0 V_p M_d |\mathbf{H}|}{kT} \quad (2)$$

$$\mu_0 (\mathbf{M} \cdot \nabla) \mathbf{H} + 2\zeta \nabla \times \boldsymbol{\omega} + (\zeta + \eta) \nabla^2 \mathbf{v} = 0 \quad (3)$$

$$\mu_0 (\mathbf{M} \times \mathbf{H}) + 2\zeta (\nabla \times \mathbf{v} - 2\boldsymbol{\omega}) = 0 \quad (4)$$

$$\frac{\partial \mathbf{M}}{\partial t} + \mathbf{v} \cdot \nabla \mathbf{M} - \boldsymbol{\omega} \times \mathbf{M} + (\mathbf{M} - \mathbf{M}_{eq})/\tau = 0 \quad (5)$$

For the simplified expressions of (3) and (4), the fluid linear flow velocity vector is \mathbf{v} , the magnetic fluid spin-velocity vector is $\boldsymbol{\omega}$, η is the dynamic shear viscosity of the ferrofluid in $\text{N}\cdot\text{s}\cdot\text{m}^{-2}$, measured as 0.002 by Elborai when $\phi = 0.035$ [13], ζ is the ferrofluid vortex viscosity

in $\text{N}\cdot\text{s}\cdot\text{m}^{-2}$, given by $\frac{3\eta\phi}{2}$ for $\phi \ll 1$, and the $\mu_0(\mathbf{M} \times \mathbf{H})$ term is the magnetic torque density given in $\text{N}\cdot\text{m}^{-2}$. The expressions consider the situation of sinusoidal steady state with viscous dominated flow conditions (so that inertia is negligible) and the magnetic fluid only responds to force and torque densities which have time-averaged, non-zero components. Also set to zero are the coefficients of shear and bulk viscosity (η' and λ') [1] discussed by Elborai [13] and He [14]. It will be apparent that in the case of immobilized nanoparticles (*e.g.*, particles attached to a tumor), there will be no flow, *i.e.*, $\mathbf{v} = \mathbf{0}$.

Magnetic relaxation of the superparamagnetic nanoparticles is governed by Shliomis' Relaxation Equation, given by (5) where \mathbf{M} is the instantaneous fluid magnetization and the magnetic fluid relaxation time [1] is τ , given by (6). The time constant's dependence on nanoparticle radius [1,15] is plotted in Figure 1.

$$\frac{1}{\tau} = \frac{1}{\tau_B} + \frac{1}{\tau_N} \quad (6)$$

As seen from (6), τ , is due to two distinct contributions. These are the Brownian (τ_B) and Néel (τ_N) relaxation times. For Brownian relaxation, which dominates at larger particle sizes, relaxation is due to particle rotation in the carrier liquid. For Néel relaxation, which is the dominant mechanism for smaller particle sizes (≤ 5 nm), the mechanism is due to rotation of the magnetic vector within the particle. If the nanoparticle is constrained, for example by attaching it to a tumor surface, Néel relaxation is still operative although Brownian is not. Therefore, in the context of hyperthermia treatment, it is the Néel relaxation which accounts for the majority of the therapeutic effect. The relative expressions for τ_B and τ_N are given by (7) and (8) respectively where V_h is the nanoparticle hydrodynamic volume in m^3 (including the surfactant contribution), η is the dynamic viscosity of the carrier liquid (assumed that of water in this analysis) in $\text{Pa}\cdot\text{s}$, k is Boltzmann's constant ($1.38 \times 10^{-23} \text{ m}^2\cdot\text{kg}\cdot\text{s}^{-2}\cdot\text{K}^{-1}$), T is the absolute temperature in K (assumed $310 \text{ K} = 37^\circ\text{C}$ unless stated), V_p is the nanoparticle volume in m^3 (excluding surfactant contribution), K_a is the anisotropy constant in J m^{-3} (with a value of 46.8×10^3 for magnetite [16]) and τ_0 is the characteristic Néel time given by Rosensweig [1] as 1 ns. For hyperthermia applications, the surfactant serves two purposes. The first is the prevention of agglomeration and the second is the functionalization of the nanoparticle. Surfactant thicknesses up to double the core radius are not uncommon.

$$\tau_B = \frac{3V_h\eta}{kT} \quad (7)$$

$$\tau_N = \tau_0 e^{\frac{K_a V_p}{kT}} \quad (8)$$

Complex notation is employed for convenience where the complete field solutions to (3) through (5) have sinusoidal time variation as given by (9) through (11) and \hat{i}_x , \hat{i}_y and \hat{i}_z are the unit vectors in a rectangular coordinate system. To facilitate analytical solutions, consider the x and z -directed magnetic fields to be applied by means of z and x -directed planar surface current sources at $y = 0$, d respectively in a planar channel of width d along y , and of infinite extent in x and z . In this case, the magnetic fields are not functions of x and z , but, at most, only a function of y . However, since the magnetic field in a current-free media has a curl $\nabla \times \mathbf{H} = \mathbf{0}$ from Ampere's Law, and the magnetic flux density obeys Gauss' Law (*i.e.*, $\nabla \cdot \mathbf{B} = \mathbf{0}$), we

find that in uniform applied DC magnetic fields, B_0 , H_0 and M_0 are all uniform while h_x and b_y are independent of y .

In a realistic MRI/hyperthermia system, the transverse field might be applied by means of birdcage or planar current-driven coil and the z -directed DC field is the B_0 field of the MRI. However, the resulting fluid magnetization and associated spin-velocity are not analytically solvable. Therefore, the notion of a planar channel is introduced for convenience to facilitate analytical solutions.

$$\mathbf{M} = \Re e\{(\widehat{m}_x(y)\mathbf{i}_x + \widehat{m}_y(y)\mathbf{i}_y)e^{j\Omega t}\} + M_0\mathbf{i}_z \quad (9)$$

$$\mathbf{H} = \Re e\{(\widehat{h}_x\mathbf{i}_x + \widehat{h}_y(y)\mathbf{i}_y)e^{j\Omega t}\} + H_0\mathbf{i}_z \quad (10)$$

$$\mathbf{B} = \Re e\{(\widehat{b}_x(y)\mathbf{i}_x + \widehat{b}_y\mathbf{i}_y)e^{j\Omega t}\} + B_0\mathbf{i}_z \quad (11)$$

In the absence of any applied pressure differential or imposed linear flow ($\mathbf{v} = 0$), the solutions of (5) for the x and y directed transverse magnetization components, associated with the applied transverse rotating field are given by (12) and (13) [15].

$$\widehat{m}_x = \frac{M_0}{H_0} \frac{(j\Omega\tau + 1 + M_0/H_0)\widehat{h}_x - (\omega_z\tau)\widehat{b}_y/\mu_0}{(j\Omega\tau + 1)(j\Omega\tau + 1 + M_0/H_0) + (\omega_z\tau)^2} \quad (12)$$

$$\widehat{m}_y = \frac{M_0}{H_0} \frac{(\omega_z\tau)\widehat{h}_x + (j\Omega\tau + 1)\widehat{b}_y/\mu_0}{(j\Omega\tau + 1)(j\Omega\tau + 1 + M_0/H_0) + (\omega_z\tau)^2} \quad (13)$$

In the limit of very low frequency excitation ($\Omega\tau \ll 1$) and zero spin-velocity ($\omega_z\tau \sim 0$), the transverse xy magnetization components, \widehat{m}_x and \widehat{m}_y , are related to the fields causing them (*i.e.*, h_x and b_y respectively) by M_0/H_0 as indicated in (14) since for all practical values of MRI field strength (*e.g.*, $\mu_0 H_0 \geq 0.1$ T), the DC magnetization is much less than the source DC field, $M_0 \ll H_0$.

$$\begin{aligned} \widehat{m}_x &\approx \frac{M_0}{H_0} h_x \\ \widehat{m}_y &\approx \frac{M_0}{H_0} \frac{b_y}{\mu_0} \end{aligned} \quad (14)$$

The spin-velocity, $\boldsymbol{\omega}$, shown in the expressions of (12) and (13) was solved in the absence of imposed flow ($\mathbf{v} = 0$) by analysis of the conservation of angular (4) and linear momentum (3) with the solution being z -directed ($\boldsymbol{\omega} = \omega_z\mathbf{i}_z$) and given by (15) [1,15]. In the thermodynamic analysis which follows there is no imposed flow.

$$\omega_z = \frac{1}{8\zeta} \Re e(\widehat{m}_x\widehat{b}_y^* - \mu_0(\widehat{h}_x + \widehat{m}_x)\widehat{m}_y^*) \quad (15)$$

Since \hat{b}_y and \hat{h}_x are known imposed source terms, (12), (13) and (15) can be solved for the transverse magnetization complex amplitudes, \hat{m}_x and \hat{m}_y , considering the relationship of (16) where $\mu_0 = 4\pi \times 10^{-7}$, the magnetic permeability of free space.

$$\mathbf{B} = \mu_0(\mathbf{H} + \mathbf{M}) \quad (16)$$

2.2 Thermodynamics of Magnetic Fluids

From the first law of thermodynamics, the differential internal heat density, dU (which is independent of process path) for a closed system of constant density is given by (17) where δQ is the differential energy input and δW is the differential work done on the system. Both δQ and δW are process path-dependent, leading to the partial derivative notation.

$$dU = \delta Q + \delta W \quad (17)$$

For an adiabatic process, it can be assumed that δQ is zero so that all generated heat remains within the system. This ignores, for example, blood perfusion.

$$dU = \delta W \quad (18)$$

The internal energy is then given by δW , which, for a magnetic fluid with negligible conductivity is given by (19) [1].

$$\delta W = \mathbf{H} \cdot d\mathbf{B} \quad (19)$$

$$\delta W = \mathbf{H} \cdot d(\mathbf{H} + \mathbf{M}) \quad (20)$$

$$\delta W = \mu_0(\mathbf{H} \cdot d\mathbf{H} + \mathbf{H} \cdot d\mathbf{M}) \quad (21)$$

For cyclic variations in \mathbf{H} and \mathbf{M} , the cyclic increase in work done, ΔW , which is equal to the cyclic increase in internal energy per unit volume, ΔU is then given by integration.

$$\begin{aligned} \Rightarrow \Delta U = \Delta W &= \oint \delta W \\ \Rightarrow \Delta U &= \oint (\mathbf{H} \cdot d\mathbf{H} + \mathbf{H} \cdot d\mathbf{M}) \end{aligned} \quad (22)$$

The first term on the right side of (22) is zero for cyclic variations in \mathbf{H} while the second term on the right side can be rewritten using the Chain Rule of Differentiation.

$$\Delta U = \mu_0 \oint d(\mathbf{M} \cdot \mathbf{H}) - \mu_0 \oint \mathbf{M} \cdot d\mathbf{H} \quad (23)$$

Again, the first term on the right side is zero for cyclic variations in \mathbf{M} and \mathbf{H} so that ΔU is given by (24).

$$\Delta U = -\mu_0 \oint (\mathbf{M} \cdot d\mathbf{H}) \quad (24)$$

As noted by Rosensweig [2], ΔU is positive in a magnetic fluid solution when \mathbf{M} lags behind \mathbf{H} as occurs when the alternating-sinusoidal or rotating field frequency is such that $\Omega\tau \sim 1$. The solution is expressed in terms of one complete time period $P = 2\pi/\Omega$, in (25) for time-averaged heating. It is noted that the partial time derivative of (25) is correct for a stationary medium.

$$\langle \Delta U \rangle = -\mu_0 \int_0^P (\mathbf{M} \cdot \frac{\partial \mathbf{H}}{\partial t}) dt \quad (25)$$

The expression of (25) is evaluated where \mathbf{M} is the vector whose components are the complex amplitudes, \hat{m}_x and \hat{m}_y , given by (12) and (13). The time derivative of the \mathbf{H} field is evaluated in (27) where \mathbf{H} is given by (26).

$$\begin{aligned} \mathbf{H} &= \Re e \left(e^{j\Omega t} (\hat{h}_x \mathbf{i}_x + \hat{h}_y \mathbf{i}_y) \right) + H_0 \mathbf{i}_z \\ \frac{\partial \mathbf{H}}{\partial t} &= \Re e \left(j\Omega e^{j\Omega t} (\hat{h}_x \mathbf{i}_x + \hat{h}_y \mathbf{i}_y) \right) \end{aligned} \quad (26)$$

$$= \Re e \left(j\Omega e^{j\Omega t} (\hat{h}_x \mathbf{i}_x + (\hat{b}_y/\mu_0 - \hat{m}_y) \mathbf{i}_y) \right) \quad (27)$$

Substituting the expression of (27) and the transverse components of \mathbf{M} into (25) eventually yields (31). There can be no contribution from the z-directed components since they do not vary with time.

$$\langle \Delta U \rangle = -\frac{\mu_0}{2} \int_0^P \Re e \left((\hat{m}_x \mathbf{i}_x + \hat{m}_y \mathbf{i}_y) e^{j\Omega t} \cdot \{ j\Omega e^{j\Omega t} (\hat{h}_x \mathbf{i}_x + (\hat{b}_y/\mu_0 - \hat{m}_y) \mathbf{i}_y) \}^* \right) dt \quad (28)$$

$$= -\frac{\mu_0}{2} \Re e \left(\int_0^P (\hat{m}_x (j\Omega \hat{h}_x)^* + \hat{m}_y (j\Omega (\hat{b}_y/\mu_0 - \hat{m}_y))^*) dt \right) \quad (29)$$

$$= -\frac{\mu_0}{2} \Re e \left(\int_0^P (\hat{m}_x (-j\Omega \hat{h}_x^*) + \hat{m}_y (-j\Omega (\hat{b}_y^*/\mu_0 - \hat{m}_y^*))) dt \right) \quad (30)$$

$$= \frac{\mu_0}{2} \Re e \left(j\Omega \hat{m}_x \hat{h}_x^* + j\Omega \hat{m}_y (\hat{b}_y^*/\mu_0) \right) P \quad (31)$$

The last term of (30) contains \hat{m}_y multiplied by its complex conjugate (purely real) which is then multiplied by j so this term is purely imaginary and thus has no real part. It is eliminated from the expression in (31). The period P , is given by $2\pi/\Omega$ so further simplification is possible.

$$\langle \Delta U \rangle = \mu_0 \Re \left(j\pi (\widehat{m}_x \widehat{h}_x^* + \widehat{m}_y (\widehat{b}_y^* / \mu_0)) \right) \quad (32)$$

Substituting for $\widehat{h}_x = H_e$ and $\widehat{b}_y = jB_e$ where H_e and B_e are real-valued quantities leads to (33), generating a rotating field in the transverse xy plane. For a purely alternating-sinusoidal field, we allow the y component to be zero (*i.e.*, $\widehat{b}_y = 0$). In the case of a rotating field in the transverse plane, B_e and H_e are the imposed y and x field components respectively and in this analysis they are related by $B_e = \mu_0 H_e$.

$$\langle \Delta U \rangle = \mu_0 \Re \left(j\pi (\widehat{m}_x H_e + \widehat{m}_y (-jB_e / \mu_0)) \right) \quad (33)$$

The volumetric, time-averaged, power dissipation, P_v , in W/m^3 is then given by $P_v = \Omega \langle \Delta U \rangle / (2\pi)$ as shown in (34). This expression equals equation (6) of Rosensweig's work [2] when B_e is zero and the spin velocity in (12) and (13) is ignored.

$$P_v = \mu_0 \Re \left(\frac{j\Omega}{2} (\widehat{m}_x H_e + \widehat{m}_y (-jB_e / \mu_0)) \right) \quad (34)$$

While Rosensweig related this expression to the rate of temperature rise, the specific absorption rate (SAR) is the conventional measure of heating effects in human tissue. SAR is given by the volumetric power dissipation divided by the mass density, ρ_m , in kg/m^3 , as in (35). As noted by Andra et al. [18], the value of ρ_m should be given by the mass of magnetic nanoparticles per unit mass of tissue rather than the value of the tissue mass density.

$$SAR = P_v / \rho_m = \mu_0 \Re \left(\frac{j\Omega}{2\rho_m} (\widehat{m}_x H_e + \widehat{m}_y (-jB_e / \mu_0)) \right) \quad (35)$$

The relation between SAR and temperature rise *in vivo* has been evaluated by Andra [18] using the result of Carslaw [3] for the particular case of a small, spherical tumor in relatively homogenous tissue with low blood perfusion (*e.g.*, muscle tissue or fat). Carslaw derives and states the radial and temporal dependencies inside ($r < R$) and outside ($r > R$) a sphere of radius R containing a uniform power dissipation source, P_v for $r < R$. In this work, P_v is due to the time-averaged power dissipation of the magnetic nanoparticles in the transverse magnetic field. The situation is approximately realized in breast tumors. While the full expressions ([3], pp. 232) detail spatial and temporal variations in temperature, the steady-state temperature rise above ambient temperature, ΔT , on the surface of a spherical tumor of radius, R , is given by (36) where λ is the heat conductivity of tissue with an approximate value of $0.64 \text{ W}\cdot\text{K}^{-1}\cdot\text{m}^{-1}$ [18].

$$\Delta T = \frac{SAR \cdot R^2 \rho_m}{3\lambda} = \frac{P_v R^2}{3\lambda} \quad (36)$$

The variation in the steady-state temperature rise is investigated for a number of cases of interest. The work represents two significant developments over that of Rosensweig [2]. Firstly, the case of rotating rather than purely alternating-sinusoidal magnetic field excitation is investigated. Secondly, the effect of excitation, with both sinusoidal and rotating fields, is investigated in the presence of a low-field 0.2 T MRI system. The rotating and sinusoidal fields are applied orthogonal to the DC $B_0 \approx \mu_0 H_0$ field. In each case, the effect of variation in (i)

particle radius, r , (ii) field amplitude, $H_e = B_e/\mu_0$ and (iii) solid magnetic volume fraction, ϕ , is investigated. In estimating ΔT on the tumor surface, the magnetic mass density is given by $\rho_m = \rho_{Fe_3O_4}\phi$ where the density of magnetite, $\rho_{Fe_3O_4}$, has a value of 5180 kg/m^3 [2].

3 Results

3.1 Alternating-Sinusoidal Field Excitation in the absence of MRI

This section examines heating in the absence of MRI with an alternating-sinusoidal magnetic field excitation. Following the analysis of Rosensweig, spin-velocity is zero (*i.e.*, $\omega_z = 0$) in the case of an alternating-sinusoidal driving magnetic field. This leads to a simplification in the expressions for \hat{m}_x and \hat{m}_y in (12) and (13) as given by (37) and (38) where the sinusoidal excitation has amplitude H_e and is applied along the x direction. The orthogonal flux-density along y , with amplitude B_e , is set to zero.

$$\hat{m}_x = \chi \frac{\hat{h}_x}{(j\Omega\tau + 1)} \quad (37)$$

$$\hat{m}_y = 0 \quad (38)$$

Following Rosensweig's formulation, the actual susceptibility is field-dependent and therefore, also time-dependent when the field is time-varying. In the absence of the B_0 field characteristic of MRI, the only field is the alternating-sinusoidal field with amplitude, H_e . The field-dependent susceptibility, (denoted χ_0 by Rosensweig) is given by (39) [1] using the chord susceptibility employed by Rosensweig. In reality, this is the maximum value of the chord susceptibility, corresponding to points in time when the instantaneous sinusoidal magnetic field is H_e . So the magnetic saturation effects predicted using this value may overestimate those observed in experiment.

$$\chi = \frac{\phi M_d}{H_e} (\coth(\alpha) - 1/\alpha) \quad (39)$$

The field-dependent susceptibility, χ is plotted in Figure 2 as a function of particle radius for various values of field excitation, denoted H_e , in units of A/m. Clearly, as particle radius increases, the field-dependent susceptibility, increases. As already noted, in the absence of the MRI's B_0 field, the magnetic field dependence is not on B_0 (which is zero for now) but on the amplitude of the alternating-sinusoidal or rotating field, denoted H_e in each case. As H_e increases, the susceptibility, decreases as the fluid slowly approaches magnetic saturation due to H_e . This is apparent in Figure 2 where, for any particular particle radius, an increasing H_e results in decreased susceptibility. The peak value (*i.e.*, corresponding to the instantaneous alternating sinusoidal field being equal to H_e) of the unitless Langevin parameter is

$$\alpha = \frac{\mu_0 V_p M_d H_e}{kT} \text{ in this case and all other quantities are as noted in relation to (1) and (2).}$$

The change in steady state temperature rise, ΔT , on the surface of a tumor of radius $R = 1 \text{ cm}$ is shown versus nanoparticle radius for changing values of particle concentration, ϕ , and $\mu_0 H_e = 10 \text{ mT}$ in Figure 4(a). It is assumed that all nanoparticles are confined within the tumor ($r < R$) and are uniformly distributed with solid volume fraction, ϕ . While this represents a considerable simplification on the reality, it serves to illustrate the potential effect. The steady state temperature rise is shown in Figure 5(a) for changing values of field amplitude, H_e , and

$\phi = 0.005$. The applied field frequency is 1.88×10^6 rad/s or 300 kHz in each case. Tissue was assumed to have the same mass density as water at room temperature (998 kg/m^3) and, unlike in Rosensweig's approach [2], the magnetic fluid suspension was assumed water-based. The surfactant thickness was taken as 10 nm throughout.

3.2 Alternating-Sinusoidal Field Excitation in the presence of MRI

This section examines the effect of heating due to an alternating-sinusoidal magnetic field in the presence of the B_0 field of MRI. In the MRI, the large, z -directed B_0 field is applied in addition to the transverse x -directed sinusoidal magnetic field. The primary effect of B_0 on the magnetic fluid's magnetization is that the saturation of the nanoparticles is determined primarily by B_0 when $B_0 \gg \mu_0 H_e$. Since physically achievable alternating-sinusoidal or rotating fields are unlikely to exceed tens of mT [4] due to power requirements, the assumption that saturation is determined by B_0 is reasonable for B_0 in the range of 0.1 T to 0.35 T. The expressions for the complex magnetization amplitudes \tilde{m}_x and \tilde{m}_y are identical to that of (37) and (38) where $\omega_z = 0$ in the absence of a y component of magnetic field. Also, χ is replaced by M_0/H_0 and M_0 is given by (1) while $|\mathbf{H}| = H_0$ is approximately given by B_0/μ_0 for the B_0 fields considered in this work since $H_0 \gg M_0$. The ratio of M_0/H_0 is plotted in Figure 3 versus the particle radius for three values of B_0 which are of interest. Clearly, as B_0 increases, the ratio of M_0/H_0 decreases in value.

The change in steady state temperature rise, ΔT , on the surface of a tumor of 1 cm radius is shown versus nanoparticle radius for changing values of particle concentration, ϕ , and $\mu_0 H_e = 10$ mT in Figure 4(b) for an MRI field strength of 0.2 T. The steady state temperature rise is shown in Figure 5(b) for changing values of field amplitude, H_e , $\phi = 0.005$ and $B_0 = 0.2$ T. Again, the applied field frequency is 1.88×10^6 rad/s or 300 kHz in each case and the surfactant thickness was taken as 10 nm.

3.3 Rotating Field Excitation in the presence of MRI

The alternating-sinusoidal field of the previous section is now replaced by a rotating field of amplitude H_e and frequency of 1.88×10^6 rad/s or 300 kHz. The rotating field is generated by means of an imposed, y -directed flux density of magnitude $B_e = \mu_0 H_e$, which is temporally displaced by a quarter time period from the x component. The z -directed $B_0 = 0.2$ T field is maintained. The results are shown in Figure 4(c) for $\mu_0 H_e = 10$ mT with changing ϕ and Figure 5(c) for $\phi = 0.005$ with changing H_e . The tumor radius is again assumed to be 1 cm. The expressions for the transverse complex magnetization amplitudes are identically (12) and (13) where it is assumed that saturation is determined primarily by the B_0 field and not the transverse rotating field amplitude. Spin velocity is non-zero in this case and given by (15).

4 Discussion

4.1 Alternating-Sinusoidal Field Excitation in the absence of MRI

Figure 4(a) and Figure 5(a) complement those of Rosensweig although the solution is now a water-based rather than an hydrocarbon-based (tetradecane) solution [2] as was the case in Rosensweig's analysis. The time constant, τ , as plotted in Figure 1, varies with particle radius as shown in Figure 1. In the case of a constrained nanoparticle (such as the case of a particle which is bound to a tumor site) Néel relaxation is expected to dominate. Therefore, for the results of Figure 4 and Figure 5, the Brownian relaxation time in infinite ($\tau_B \rightarrow \infty$) and $\tau_N = \tau$.

As is evident from Figure 4 and Figure 5 the steady-state temperature rise is a maximum at a particle radius of approximately 5nm for a rotating field frequency of 300 kHz. As one might suspect from the expressions of (12) and (13), this is where the product of $\Omega\tau$ approaches unity

when $\Omega = 1.88 \times 10^6$ rad/s or 300 kHz. This is true for both alternating-sinusoidal and rotating fields and is true regardless of the presence of the MRI's B_0 field.

4.2 Alternating-Sinusoidal Field Excitation in the presence of MRI

After the addition of the z -directed B_0 field which characterizes MRI, the most striking result is the large decrease in ΔT . This is because, for reasons of practical realizability, B_0 is chosen to dominate the sinusoidal or rotating field amplitude, $\mu_0 H_e$, throughout this work. This decrease is greater as B_0 increases. The presence of B_0 causes the fluid to approach saturation far more rapidly than occurs in the presence of the rotating field. Saturation impedes nanoparticle rotation, and hence, heat generation, since one can imagine that as a larger fraction of the nanoparticles remain saturated, their magnetic moments remain collinear with B_0 and do not respond to the sinusoidal field excitation orthogonal to B_0 , along the x axis. This result is supported by comparing plots (a) and (b) of Figure 4 and Figure 5. Since the DC B_0 field itself does not add or subtract heat from the fluid, the dramatic change in heating can only be accounted for by the partial magnetic saturation which occurs in its presence.

ΔT will increase linearly in the presence of B_0 although the dependence on H_e is non-linear as seen in Figure 5.

4.3 Rotating Field Excitation in the presence of MRI

Adding a second orthogonal field component to the previous case of an alternating-sinusoidal field has the effect of creating a rotating field if the two components are temporally displaced by a quarter cycle. The results take account of the spin-velocity in the ferrofluid although the effects of spin-velocity only become significant in narrow channels (μm) or with large, imposed channel flow velocities (≥ 10 m/s) [15]. The term is nonetheless included for completeness. Therefore, the results for a rotating field in addition to the MRI's B_0 field show an approximate factor of two increase in ΔT , as might be expected, compared to the case of a purely alternating-sinusoidal field albeit at the cost of a second RF power amplifier for the y component of the rotating field.

5 Conclusions

This paper examines the potential for magnetic nanoparticle hyperthermia in low-field MRI (0.2 T) where the nanoparticles are still free to rotate due to incomplete magnetic saturation, as determined by the Langevin function. The conclusion of the analysis is that, perhaps contrary to intuition, significant nanoparticle heating is still conceivable, due to Néel relaxation effects, even at 0.2 T MRI field strength. Nanoparticles with a magnetic core radius corresponding to $\Omega\tau = 1$ show the most significant effect. This is clear from the results in Figure 4 and Figure 5 where, although the steady-state temperature increase in a 1 cm radius spherical tumor (assuming no perfusion) is decreased significantly by the addition of the MRI field, temperature increases of up to 10°C are still possible with reasonable values of rotating field amplitude ($\sim 10\%$ of B_0) and particle concentration ($\phi \sim 0.01$). This is well within the range of 4°C to 7°C typical in hyperthermia treatment for breast cancer.

To the author's best knowledge, this work represents the first time that an analysis of this kind has been undertaken which bridges the rotational dynamics of magnetic nanoparticle suspensions (ferrofluids) [1,2] with two of the primary applications of these nanoparticles in modern medicine: magnetic nanoparticle hyperthermia [4–6] and MRI contrast agents. This work raises the possibility of combining these two applications in a single therapeutic environment, where, for example, magnetic nanoparticle hyperthermia for breast cancer treatment could be combined with low-field (*e.g.*, 0.2 T) MR imaging for real-time, non-invasive temperature measurement.

Acknowledgments

The authors would like to acknowledge the reviewer's insightful and informed comments which greatly improved the form and consistency of the publication.

References

1. Rosensweig, RE. Ferrohydrodynamics. New York, New York: Dover Publications; 1997.
2. Rosensweig RE. *J Magn Magn Mater* 2002;252:370–374.
3. Carslaw, HS.; Jaeger, JC. *Conduction of Heat in Solids*. Oxford, England: Oxford University Press; 1957.
4. Hergt R, Dutz S. *J Magn Magn Mater* 2007;311:187–192.
5. Hergt R, Dutz S, Muller R, Zeisberger M. *J Phys-Condens Mat* 2006;18:S2919–S2934.
6. Jordan A, Scholz R, Wurst P, Fahling H, Felix R. *J Magn Magn Mater* 1999;201:413–419.
7. Moroz P, Jones SK, Gray BN. *Int J Hypertherm* 2002;18:267–284.
8. Brezovich IA. *Med Phys Monograph* 1988;16:82–111.
9. Seo WS, Lee JH, Sun X, Suzuki Y, Mann D, Liu Z, Terashima M, Yang PC, McConnell MV, Nishimura DG, Dai H. *Nature Mater* 2006;5 971976.
10. Delannoy, J.; LeBihan, D.; Levin, RL.; Hoult, DI. *Engineering in Medicine and Biology Society, (1988). Proceedings of the Annual International Conference of the IEEE Engineering in Medicine and Biology Society; 1988. p. 344-345.*
11. Salomir R, Vimeux FC, de Zwart JA, Grenier N, Moonen CTW. *Magn Reson Med* 2000;43:342–347. [PubMed: 10725875]
12. Zahn M, Greer DR. *J Magn Magn Mater* 1995;149:165–173.
13. Elborai, SM. PhD Thesis. Massachusetts Institute of Technology; 2006.
14. He, X. PhD Thesis. Massachusetts Institute of Technology; 2006.
15. Cantillon-Murphy, P. PhD Thesis. Massachusetts Institute of Technology; 2008.
16. Goya GF, Berquó TS, Fonseca FC, Morales MP. *J App Phys* 2003;94:3520.
17. Shliomis M. *Soviet Physics JETP* 1972;34:1291.
18. Andra W, d'Amblay CG, Hergt R, Hilger I, Kaiser WA. *J Magn Magn Mater* 1999;194:197–203.

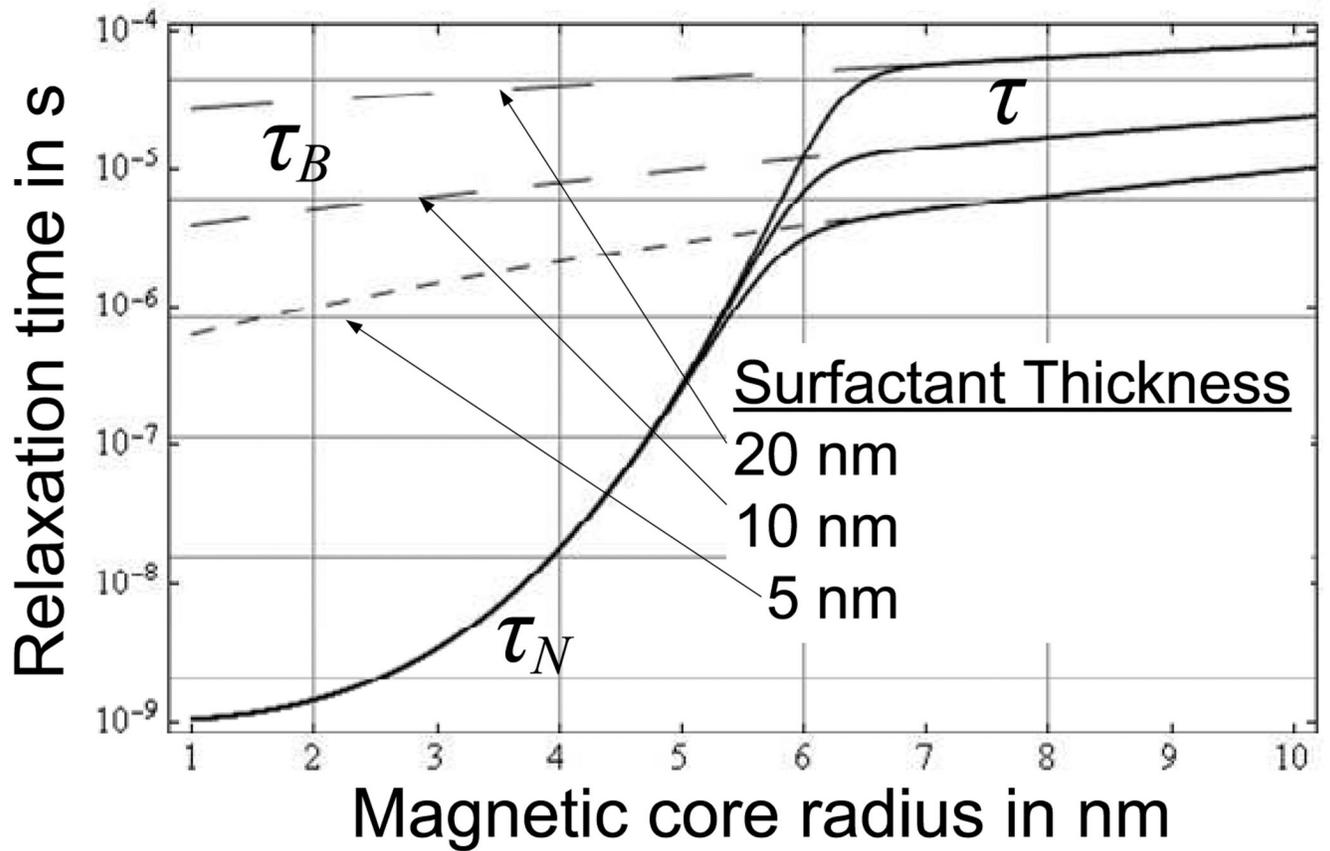


Fig. 1. The magnetic fluid time constant, τ , is usually dominated by either the Néel (τ_N) or Brownian (τ_B) relaxation times, depending on the particle's radius.

Field-dependent susceptibility for $B_0=0$

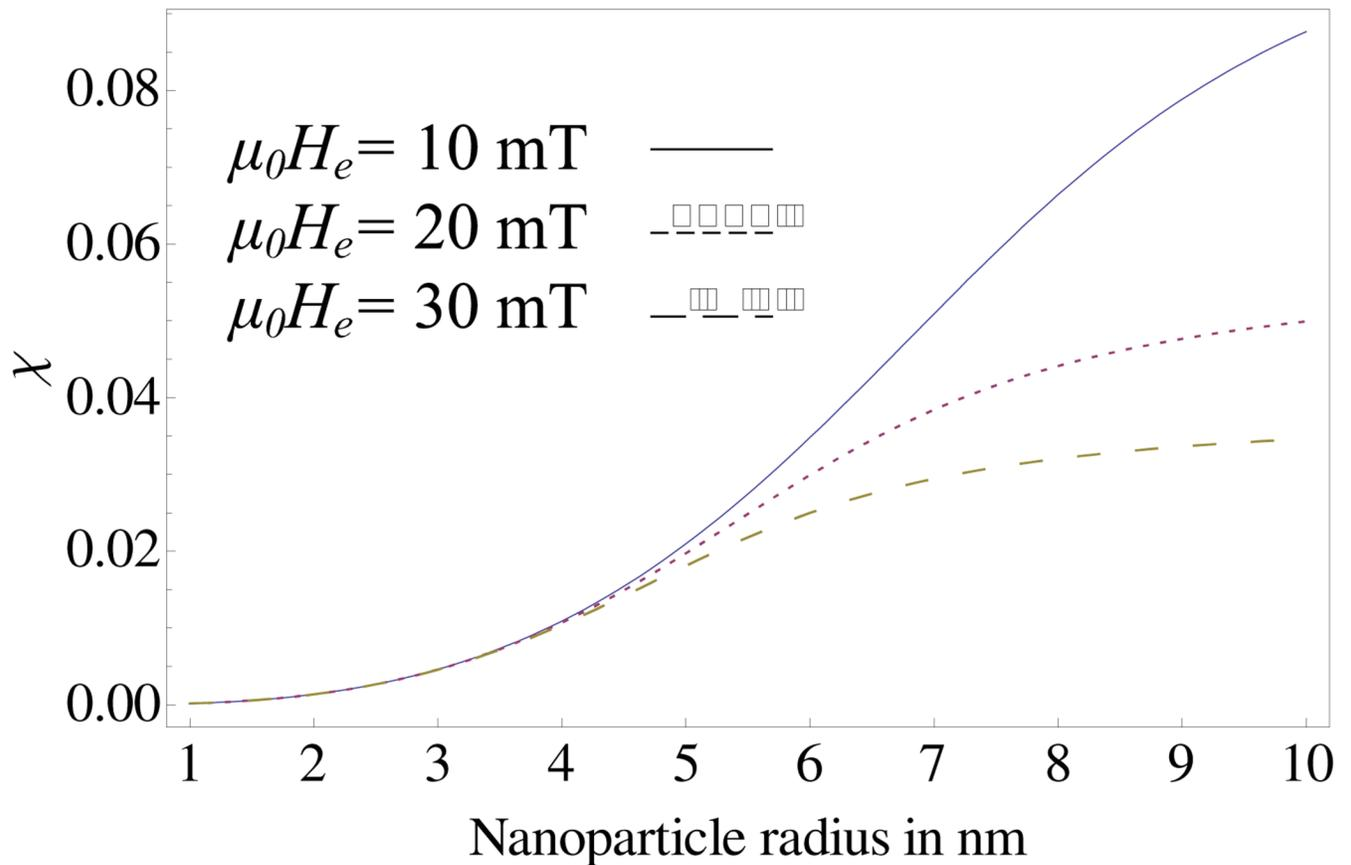


Fig. 2. The effect of particle radius on the field-dependent susceptibility in the absence of MRI, given by (39), is examined for three magnetic fields of interest: $\mu_0 H_e = 10$ mT, 20 mT and 30 mT. As the nanoparticle radius approaches 0, the susceptibility also tends towards zero. Solid volume fraction is $\phi = 0.002$ and M_d is assumed that for magnetite, $M_d = 446 \times 10^3$ A/m.

M_0/H_0 for various MRI Field Strengths

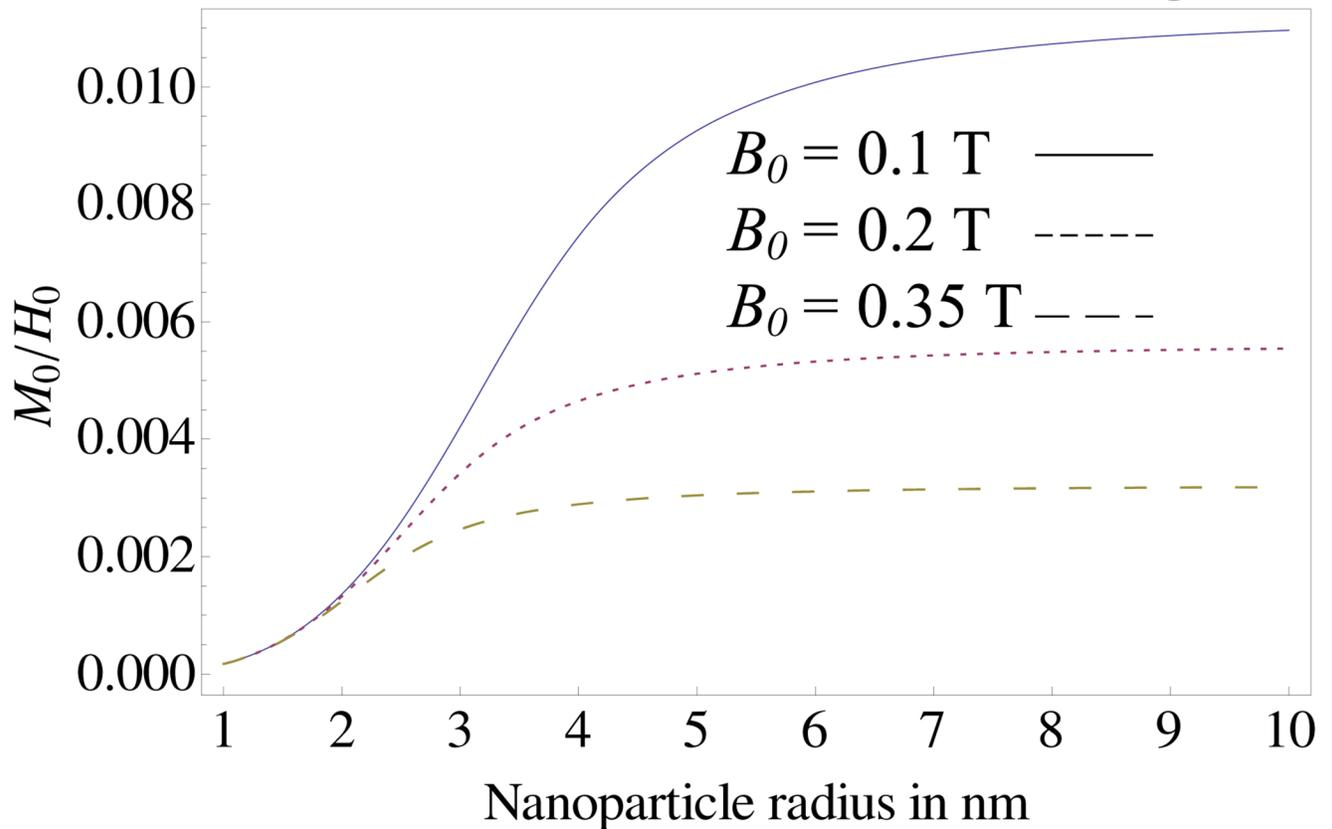


Fig. 3.

The effect of changing particle radius on the ratio of M_0 to H_0 is shown for increasing values of B_0 , 0.1 T, 0.2 T and 0.35 T. The ratio saturates at large values of r as might be expected since the onset of magnetic saturation is earlier with increasing particle size. Again, solid volume fraction is $\phi = 0.002$ and M_d is assumed that for magnetite, $M_d = 446 \times 10^3$ A/m.

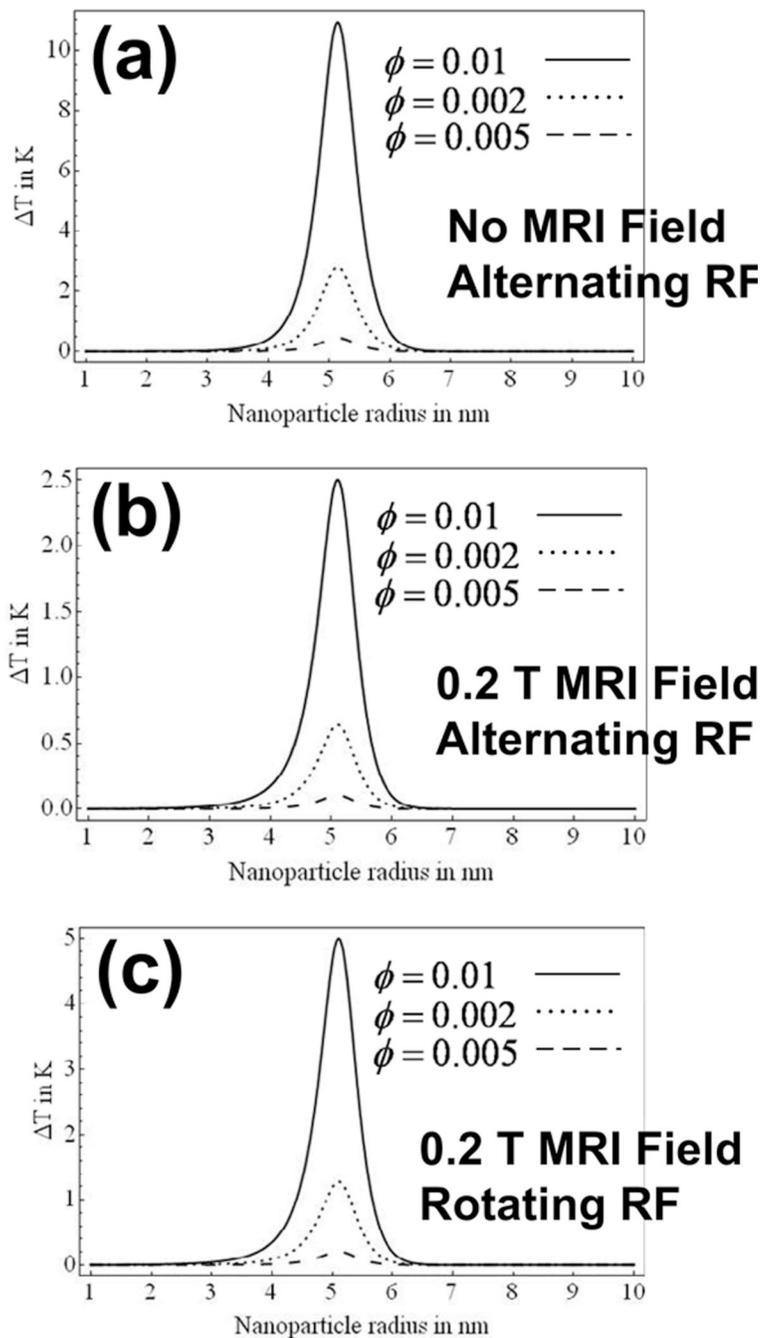


Fig. 4. The effect on ΔT is shown versus particle radius with varying magnetic nanoparticle concentration (a) without MRI due to an alternating-sinusoidal magnetic field of 10 mT, (b) with a 0.2 T MRI field and an alternating-sinusoidal magnetic field of 10 mT and, (c) with a 0.2 T MRI field magnetic and a rotating field of 10 mT. For these result, the RF frequency is 300 kHz, $\phi = 0.002$ and τ is a function of nanoparticle radius, as plotted in Figure 1. A 1 cm radius tumor is considered throughout.

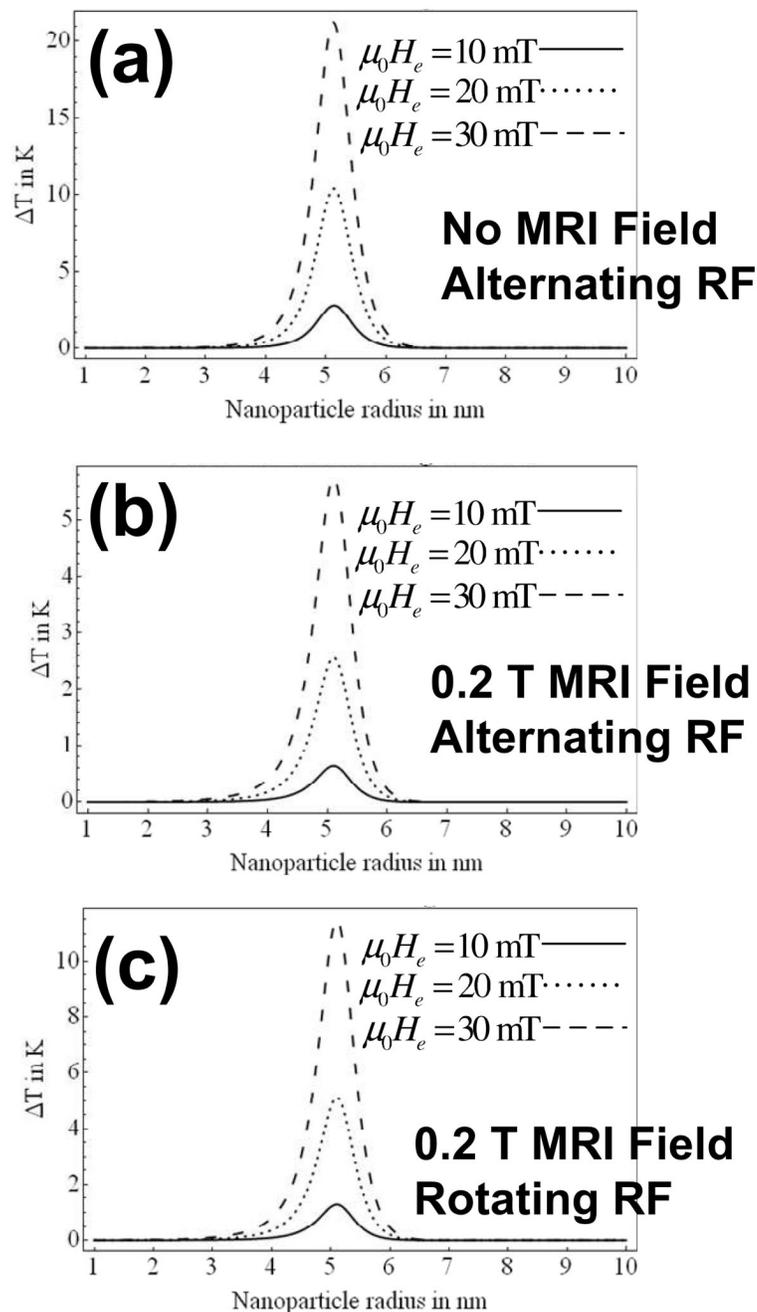


Fig. 5. The effect on ΔT is shown versus particle radius with varying magnetic field amplitudes (a) without MRI due to an alternating-sinusoidal magnetic field, (b) with a 0.2 T MRI field, an alternating-sinusoidal magnetic field, and, (c) with a 0.2 T MRI field, a rotating magnetic field. Again, the RF frequency is 300 kHz, τ is a function of nanoparticle radius, as plotted in Figure 1 and nanoparticle concentration is $\phi = 0.005$. A 1 cm radius tumor is considered throughout.